Title
A NUMERICAL STUDY OF CAPILLARY STABILITY IN A CIRCULAR CYLINDRICAL CONTAINER WITH A CONCAVE SPHEROIDAL BOTTOM

Author
Concus, P.

Publication Date
1977-02-01

To be submitted for publication

LBL-6144
Preprint

A NUMERICAL STUDY OF CAPILLARY STABILITY IN A CIRCULAR CYLINDRICAL CONTAINER WITH A CONCAVE SPHEROIDAL BOTTOM

P. Concus and I. Karasalo

February 1977

Prepared for the U. S. Energy Research and Development Administration under Contract W-7405-ENG-48

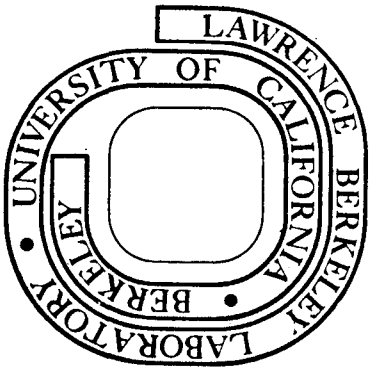

DISCLAIMER

A NUMERICAL STUDY OF CAPILLARY STABILITY IN A CIRCULAR CYLINDRICAL CONTAINER WITH A CONCAVE SPHEROIDAL BOTTOM

P. Concus*

I. Karasalo**

February, 1977

ABSTRACT

We study computationally the stability, under gravitational and surface forces, of a liquid in a circular cylindrical container with a concave spheroidal bottom, for the case in which the volume of liquid is sufficiently small so that the bottom is not covered entirely. We assume the gravitational field to be directed along the axis of symmetry of the container, and for a specific container shape we compute the critical Bond number as a function of liquid volume for contact angles $\gamma = 0°$, $1°$, $2°$, and $4°$. For the case $\gamma = 0°$ we present graphically several critical equilibrium configurations and corresponding perturbation modes.

* Lawrence Berkeley Laboratory, University of California, Berkeley, CA 94720.

**Lawrence Berkeley Laboratory, University of California, Berkeley, CA 94720. Now at KDT, ASEA, S-721 83 Västerås, Sweden.

1. STATEMENT OF THE PROBLEM

In this paper we present the results of a computational study of the stability of a liquid in a rotationally symmetric container subject to gravitational and surface forces. We consider vertical right circular cylindrical containers with concave spheroidal bottoms, for the case in which the volume of liquid is sufficiently small so that liquid lies only in an annular region of the container (Fig. 1). We are interested specifically in the case for which the contact angle γ is zero, or nearly zero, and our numerical results are obtained for a container currently used for the storage of liquid fuels in National Aeronautics and Space Administration Centaur space vehicles, for which the axial ratio of the bottom is $b/a = 0.724$.

A vertical section through the axis of the container is depicted in Fig. 1, along with the associated cylindrical coordinate system. The container may be in motion, but the net external gravitational force is assumed to be uniform and directed parallel to the axis of symmetry. It is well known, that even if the gravitational force is directed upward, liquid may be in stable equilibrium at the container bottom because of the effect of surface forces. For a given liquid volume, stable configurations of this kind are possible only if the magnitude of the upward-directed gravitational force does not exceed a certain critical value. This critical value depends on physical parameters such as the liquid-vapor surface tension coefficient, the difference in liquid and vapor densities, the liquid-container contact angle,

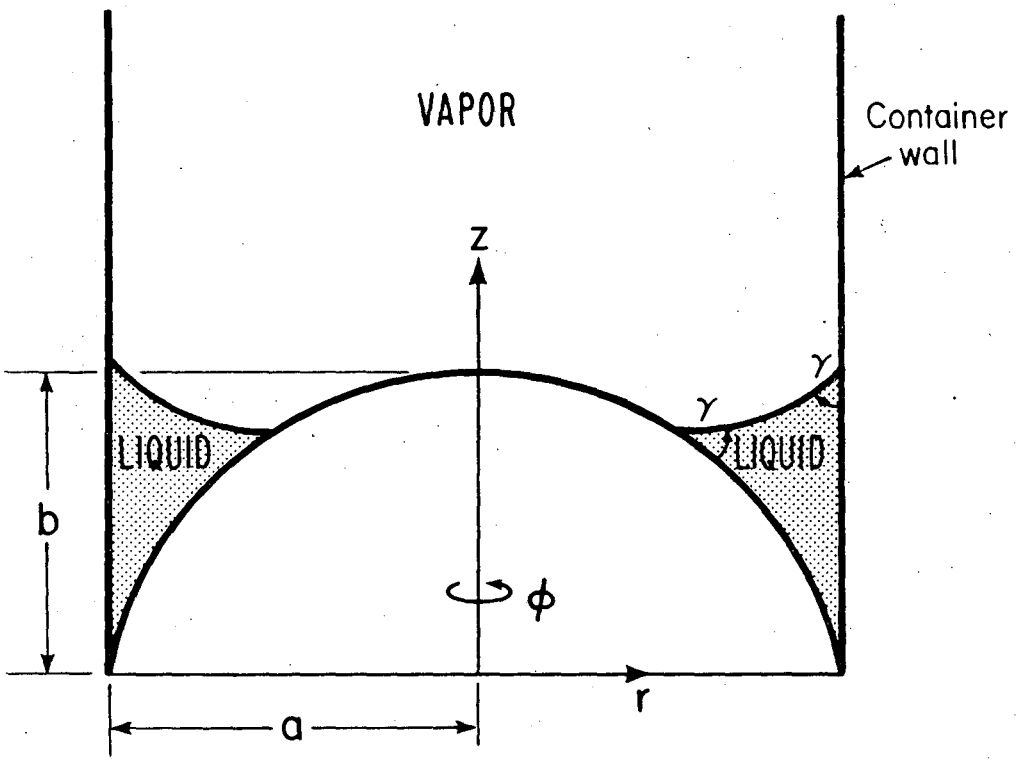

Figure 1

and geometrical parameters such as the container size and shape. The combined effect of certain of these parameters may be represented by the dimensionless Bond number (see (2.11) below), whose critical value for our problem is a function only of the container shape, the liquid volume, and the contact angle. In this study we determine computationally the critical Bond number as a function of the liquid volume for fixed contact angle and container shape.

Our approach is that of static analysis, i.e. we consider the total potential energy of the liquid-container system (in a container-fixed frame of reference), given by

$$E = \sigma(A_f - A_w \cos\gamma) + E_g \tag{1.1}$$

(cf. Reynolds and Satterlee [3], p. 394-396). Here $\sigma > 0$ (the liquid-vapor surface tension coefficient) and $0 \leqslant \gamma \leqslant \pi$ (the contact angle between the liquid vapor interface and the container wall and bottom) are constants determined by physical properties of the liquid and the container, A_f and A_w are the areas of the liquid-vapor and the liquid-container interfaces, respectively, and E_g is the gravitational potential energy of the liquid. A configuration of liquid is in stable equilibrium if and only if the total potential energy (1.1) is minimal compared with that of any nearby configuration having the same liquid volume. Thus the critical Bond number for a certain volume of liquid is the one at which E in (1.1) ceases to have a strict local minimum with respect to all perturbations that conserve the liquid volume. In Section 2 below we give a summary of an analysis of this constrained minimization problem using methods of variational calculus.

2. DERIVATION OF THE DIFFERENTIAL EQUATIONS

Because of the axial symmetry, we can restrict ourselves to consider small perturbations of initially axially symmetric configurations only (we must, however, allow for perturbations that are not axially symmetric). We use a parametric arc-length, normal-displacement representation of the surfaces (cf. Concus, Crane, and Satterlee [2], pp.4-6). Thus we let the unperturbed liquid-vapor interface be given by

$$\begin{cases} r = R(s) \\ z = Z(s) \end{cases} \qquad s_0 \leq s \leq s_1 , \quad 0 \leq \phi \leq 2\pi \tag{2.1}$$

in the cylindrical coordinate system of Fig. 1, where s is the arc-length along the curve of intersection between the unperturbed liquid-vapor interface and any plane ϕ = constant. Then the equations

$$\begin{cases} r = R(s) - \eta(s,\phi)Z'(s) \\ z = Z(s) + \eta(s,\phi)R'(s) \end{cases} \qquad s_0(\phi) \leq s \leq s_1(\phi), \quad 0 \leq \phi \leq 2\pi \tag{2.2}$$

describe a surface obtained by moving each point of the unperturbed liquid-vapor interface the distance $\eta(s,\phi)$ along the normal at (s,ϕ), cf. Fig. 2. In this way the constants s_0, s_1 and the functions $s_0(\phi)$, $s_1(\phi)$ are determined by the unperturbed liquid-vapor interface and by, respectively, the unperturbed and the perturbed three-phase contact lines. Since clearly $s_i(\phi) - s_i$, $i = 0, 1$, may assume any sign we must imagine the functions R(s) and Z(s) in (2.2) to be continued to some interval containing $s_0 \leq s \leq s_1$ in its interior, cf. the dotted

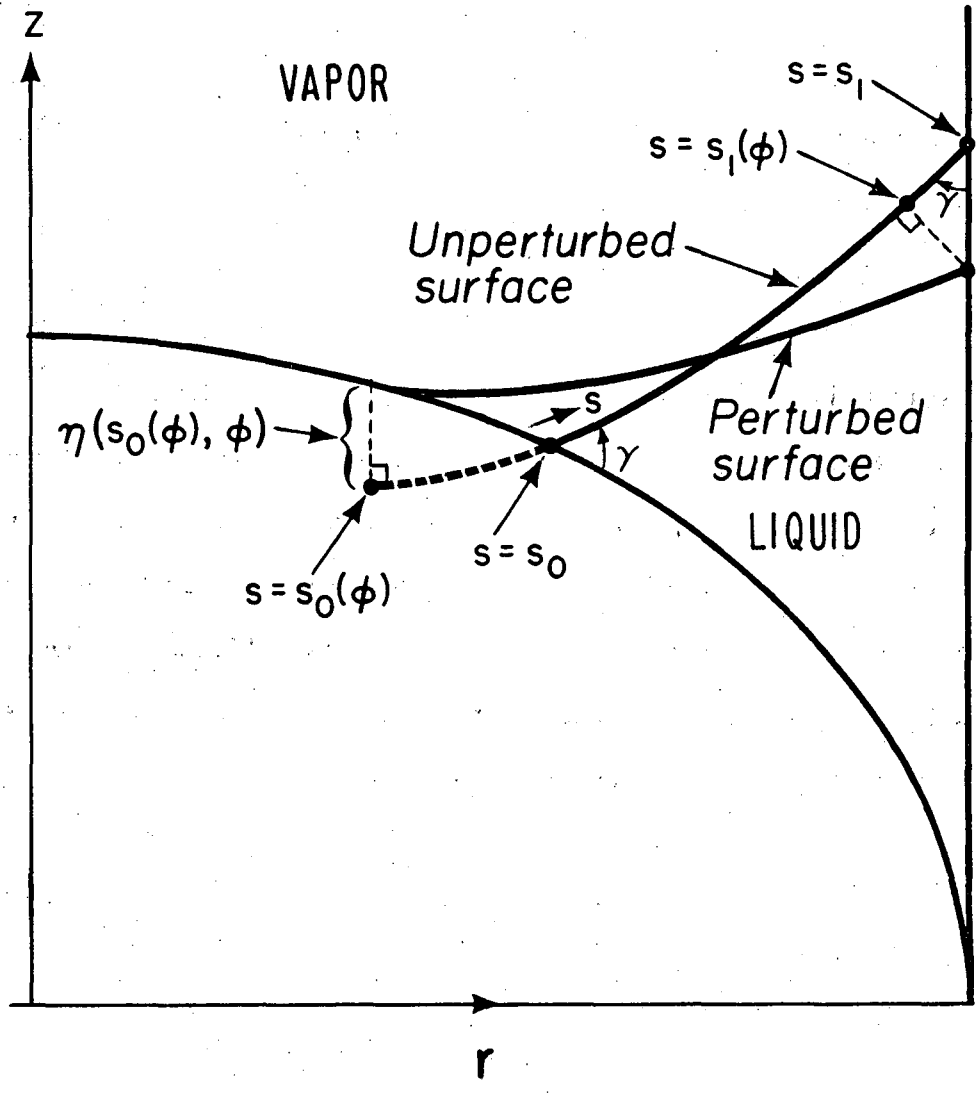

XBL 773-582

Figure 2

continuation of the unperturbed surface to the left in Fig. 2. (The continuation may be done in several ways, perhaps most conveniently by using the fact that R(s) and Z(s) will be analytic functions for equilibrium configurations, cf. (2.9) below.)

In a way similar to (2.2), the container wall and bottom are described by

$$\begin{cases} r = R(s) - w(s)Z'(s) \\ z = Z(s) + w(s)R'(s) \end{cases} \qquad 0 \leq \phi \leq 2\pi \tag{2.3}$$

in some neighborhoods of the unperturbed contact lines $s = s_0$ and $s = s_1$. Then clearly $w(s_0) = w(s_1) = 0$. The function $w(s)$ will depend on the shape of the container wall and bottom and, implicitly, the shape of the unperturbed liquid-vapor interface. The representation (2.3) is convenient for the purpose of deriving the differential equations; however, in the actual computations we must, of course, make use of the known, configuration-independent shape of the container, cf. (3.4) and (3.5) below.

The increments of the total potential energy E and the liquid volume V caused by the perturbation $\eta(s,\phi)$ in (2.2) may then be computed. We obtain in a straightforward way

$$\begin{aligned} \delta E(\eta) &= \sigma(\delta A_f - \delta A_w \cos\gamma) + \delta E_g \\ &= \int_0^{2\pi} \int_{s_0(\phi)}^{s_1(\phi)} \left\{ \sigma(f_A(\underline{\eta},s) - f_A(\underline{0},s)) + \rho g\, f_g(\underline{\eta},s) \right\} ds\, d\phi \; - \\ &\quad - \int_0^{2\pi} \int_{\Delta_\phi} \left\{ \sigma(\cos\gamma \cdot f_A(\underline{w},s) - f_A(\underline{0},s)) + \rho g\, f_g(\underline{w},s) \right\} ds\, d\phi \,, \end{aligned} \tag{2.4}$$

$$\delta V(\eta) = \int_0^{2\pi} \int_{s_0(\phi)}^{s_1(\phi)} f_V(\underline{\eta},s)\, ds\, d\phi \; - \int_0^{2\pi} \int_{\Delta_\phi} f_V(\underline{w},s)\, ds\, d\phi \,, \tag{2.5}$$

where we have put

$$\underline{\eta} = \underline{\eta}(s,\phi) = (\eta(s,\phi),\ \eta_s(s,\phi),\ \eta_\phi(s,\phi))^T \,,$$

$$\underline{w} = \underline{w}(s) = (w(s),\ w'(s),\ 0)^T \quad , \tag{2.6}$$

$$\Delta_\phi = \text{the interval } (s_0(\phi),\ s_0) \cup (s_1,\ s_1(\phi)) \,,$$

and where the functions $f_A(\underline{\eta},s)$, $f_V(\underline{\eta},s)$, and $f_g(\underline{\eta},s)$ are given by (denoting $R = R(s)$ and $Z = Z(s)$ for brevity)

$$f_A(\underline{\eta},s) = \Big\{(R - \eta Z')^2(\eta_s^2 + (1 + \eta(R''Z' - Z''R'))^2) \; + \; + \eta_\phi^2\,(1 + \eta(R''Z' - Z''R'))^2\Big\}^{\frac{1}{2}} \,,$$

$$f_V(\underline{\eta},s) = \eta\Big\{1 + \frac{\eta}{2}(R''Z' - Z''R')\Big\}(R - \frac{\eta}{2}Z') \quad ,$$

$$f_g(\underline{\eta},s) = (Z + \frac{\eta}{2}R')\, f_V(\underline{\eta},s) \,. \tag{2.7}$$

In (2.4) ρ, the liquid density (or, more precisely, the difference between the liquid and vapor densities), is assumed to be constant, and g is the gravitational constant (which may assume any value) defined so that $g > 0$ if the gravitational force pulls toward the negative z-axis.

The condition, that all first-order η-terms in $\delta E(\eta)$ as given by (2.4) should vanish for all η such that $\delta V(\eta) = 0$ in (2.5) is then

$$\sigma \frac{\partial f_A}{\partial \eta}(\underline{0},s) + \rho g \frac{\partial f_g}{\partial \eta}(\underline{0},s) - \lambda \frac{\partial f_V}{\partial \eta}(\underline{0},s) = 0$$

in $s_0 \leqslant s \leqslant s_1$, with the side-conditions (2.8)

$$\cos\gamma \cdot f_A(\underline{w}(s_i),s_i) - f_A(\underline{0},s_i) = 0,\ i = 0,\ 1,$$

where λ is a constant (the Lagrange multiplier). Putting here $B = \rho g/\sigma$, $H = \lambda/\sigma$, and using (2.7) and the identity

$$R'(s)^2 + Z'(s)^2 = 1$$

(which holds because s is the arc-length) (2.8) becomes the Euler - Lagrange boundary value problem for the equilibrium liquid-vapor interface

$$\begin{cases} R'' = -Z'(BZ - H - Z'/R) \\ Z'' = R'(BZ - H - Z'/R) \\ w(s_0) = w(s_1) = 0, \\ w'(s_0) = -\tan\gamma,\ w'(s_1) = \tan\gamma \quad . \end{cases} \tag{2.9}$$

In general, the requirement that (2.9) should have a solution for a given container shape will restrict the B, H, and V - values to some two-dimensional subset of the (B,H,V) - space.

The equations (2.9) have the following invariance property: if ℓ is any positive constant and if we put

$$\overline{R}(s) = \frac{1}{\ell} R(\ell s),\quad \overline{Z}(s) = \frac{1}{\ell} Z(\ell s),\quad \overline{w}(s) = \frac{1}{\ell} w(\ell s) \tag{2.10}$$

then $\overline{R}$ and $\overline{Z}$ will satisfy (2.9) with B replaced by $\overline{B} = B\ell^2$, H replaced by $\overline{H} = H\ell$ and w replaced by $\overline{w}$. The transformation (2.10) means simply that $\overline{R}$, $\overline{Z}$, and $\overline{w}$ describe a liquid-tank configuration obtained by uniformly enlarging the original one by a factor $1/\ell$. Therefore, if we define dimensionless constants B_0 and H_0 by

$$B_0 = B\,a^2 = \frac{a^2\rho g}{\sigma}\quad ,\quad H_0 = H\,a = \frac{a\lambda}{\sigma}\quad , \tag{2.11}$$

where a is the container radius, B_0 (the Bond number) and H_0 will be invariant under uniform re-scalings of equilibrium liquid-tank configurations. We will therefore present the results of our computations below in terms of the B_0 in (2.11) in order to facilitate their use for arbitrary-sized containers.

We assume now that the liquid-vapor interface (2.1) satisfies the Euler-Lagrange equations (2.9). Then the condition, that all second order η-terms give a non-negative contribution to $\delta E(\eta)$ in (2.4) for all η such that in (2.5) $\delta V(\eta) = 0$, may be written as

$$\int_0^{2\pi}\int_{s_0}^{s_1} \left\{ R(s)\eta_s^2 + \frac{1}{R(s)}\eta_\phi^2 + A(s)\eta^2 \right\} ds\, d\phi \; + \; + \int_0^{2\pi} \left\{ \alpha_0 \eta(s_0,\phi)^2 + \alpha_1 \eta(s_1,\phi)^2 \right\} d\phi \quad \geqslant 0 \tag{2.12}$$

for all $\eta = \eta(s,\phi)$ such that

$$\int_0^{2\pi}\int_{s_0}^{s_1} R(s)\, \eta(s,\phi)\, ds\, d\phi = 0 \quad . \tag{2.13}$$

In (2.12) we have denoted

$$A(s) = -2R'' + B\left\{RR' - ZZ' + ZR(R''Z' - Z''R')\right\} + + H\left\{Z' - R(R''Z' - Z''R')\right\} \tag{2.14}$$

and

$$\alpha_i = \frac{(-1)^i}{\tan^2\gamma} \frac{d}{ds} \left\{ \cos\gamma \cdot f_A(\underline{w}(s),s) - f_A(\underline{0},s) + B f_g(\underline{w}(s),s) - - H f_V(\underline{w}(s),s) \right\}_{s=s_i}, \quad i = 0, 1 \; . \tag{2.15}$$

It can be shown that if (2.12) (with the side-condition (2.13)) holds with strict inequality for all nonzero functions $\eta(s,\phi)$ then in fact E will be locally minimal at $\eta = 0$, i.e. the configuration described by the R(s) and Z(s) in (2.9) is a stable one. It can further be shown that if (2.12) (under (2.13)) does not hold for all η, then E cannot be locally minimal at $\eta = 0$ and the configuration is an unstable one. Thus the critical value of B will be the value at which the transition between these two cases occurs (provided that the corresponding solutions R(s), Z(s) to (2.9) describe an equilibrium liquid-vapor interface that is physically realizable, which may not always be the case - see the end of this Section). When B is critical in this sense, (2.12) still holds (under (2.13)) but there exists some non-zero $\eta = \eta(s,\phi)$ for which (2.12) holds with equality.

The inequality (2.12)-(2.13) may be analysed in terms of an associated sequence of eigenfunctions of the form

$$\{\mu_{ik}(s)\ \cos k\phi\}_{i=1,k=0}^{\infty} \tag{2.16}$$

with eigenvalues $\{\lambda_{ik}\}_{i=1,k=0}^{\infty}$. These are given by the solutions to the eigenvalue problems

$$\begin{cases} -\frac{d}{ds}\{R(s)\mu_{ik}'(s)\} + \left\{\frac{k^2}{R(s)} + A(s)\right\}\mu_{ik}(s) = \lambda_{ik}\mu_{ik}(s) \\ R(s_j)\mu_{ik}'(s_j) = (-1)^j\alpha_j\mu_{ik}(s_j) \qquad \begin{matrix} j = 0, 1 \\ k = 0, 1, 2, \ldots \\ i = 1, 2, 3, \ldots \end{matrix} \end{cases} \tag{2.17}$$

where A(s), α_0, and α_1 were introduced in (2.14)-(2.15). It can be shown from (2.17) that the eigenvalues increase with the index k. It further follows from (2.16) that all eigenfunctions but those with k = 0 in (2.16) satisfy trivially the condition (2.13). Then it follows, that (2.12) under the side-condition (2.13) holds if and only if (assuming λ_{ik} to be ordered increasingly with i)

$$\min\{\lambda_{11},\ \beta_1^2\lambda_{10} + \beta_2^2\lambda_{20}\} \geq 0 \quad , \tag{2.18}$$

where, because of (2.13), β_1 and β_2 are the solutions to

$$\begin{cases} \beta_1(\mu_{10},\ R) + \beta_2(\mu_{20},R) = 0 \\ \beta_1^2(\mu_{10},\ \mu_{10}) + \beta_2^2(\mu_{20},\mu_{20}) = 1 \ . \end{cases} \tag{2.19}$$

In (2.19) we have denoted

$$(f,g) = \int_0^{2\pi}\int_{s_0}^{s_1} f(s,\phi)\ g(s,\phi)\ ds\ d\phi \quad .$$

In all the cases studied below it will in fact hold $|(\mu_{10},\ R)| >> |(\mu_{20},\ R)|$ and $(\lambda_{20} - \lambda_{10}) >> (\lambda_{11} - \lambda_{10}) > 0$, so that the minimum in (2.18) is attained at λ_{11}. Thus, the critical value of B is determined by the condition $\lambda_{11} = 0$ (with the above mentioned restriction concerning non-realizable equilibrium configurations). By (2.14), (2.15), and (2.17), we obtain that this condition is equivalent to requiring that the Jacobi-Legendre boundary value problem

$$\begin{cases} -R\mu''(s) - R'\mu'(s) + \left\{\frac{1}{R} - 2R'' + B\{RR' - ZZ' + ZR(R''Z' - Z''R')\} + \right. \\ \qquad \left. + H\{Z' - R(R''Z' - Z''R')\}\right\}\mu(s) = 0, \quad s_0 \leq s \leq s_1 \qquad (2.20) \\ (-1)^i \tan\gamma\cdot\mu'(s_i) = \{\sin^2\gamma\cdot(R''Z' - Z''R') - \cos^2\gamma\cdot w''\}_{s=s_i}\cdot\mu(s_i) \\ \qquad i = 0, 1, \qquad (2.21) \end{cases}$$

should have a non-trivial solution $\mu(s)$.

We remark that the formulas (2.12) and (2.15) in the above discussion are meaningful only if the contact angle γ is strictly positive. However, one of our principal interests is the limiting case $\gamma = 0$. Therefore a special analysis is needed in order to determine the proper limiting form of the above conditions (2.19)-(2.20) when $\gamma \to 0$. It can be shown (Karasalo [4]) that if $w''(s_i) < 0$, $i = 0, 1$, then the differential equation (2.20) with the fixed end-point boundary conditions

$$\mu(s_0) = \mu(s_1) = 0 \qquad (2.22)$$

is the correct one to use when $\gamma = 0$. Furthermore it holds when $\gamma = 0$ that if in the set of solutions $R(s)$, $Z(s)$ to (2.9) obtained by keeping the volume fixed and varying B (and H, cf. the comment after (2.9) above) $w''(s_0)$ or $w''(s_1)$ change sign as functions of B at some value of B, then this B-value is critical even if (2.20)-(2.22) lacks nontrivial solutions. This is so because only solutions $R(s)$, $Z(s)$ for which $w''(s_0) \leq 0$ and $w''(s_1) \leq 0$ hold are permissible for $\gamma = 0$ due to the constraints imposed by the container geometry. Our computations show, in fact, for the Centaur space vehicle example, that small liquid

volumes become unstable because of the conditions (2.20)-(2.22), whereas the stability of large liquid volumes is decided by the constraint $w''(s_1) \leq 0$. The transition between these two conditions occurs at a certain well defined volume, cf. (3.6)-(3.7) below.

3. COMPUTATIONAL PROCEDURE

With a given liquid volume in a given container of the shape shown in Fig. 1 we associate a dimensionless fill height, defined as follows: let z_V be such that the given volume V coincides with the volume bounded by the container wall and bottom and the plane $z = z_V$. Then the fill height for the volume V in the container with radius a is

$$h_V = z_V/a = \frac{1}{a}\left(\frac{3b^2V}{\pi a^2}\right)^{1/3}. \tag{3.1}$$

We shall compute the critical Bond number B_{0c} (cf.(2.11)) as a function of h_V. Obviously, by (2.10)-(2.11) and (3.1), these quantities are invariant under uniform re-scalings of the container, and we can therefore restrict our computations to a container with a specific radius, e.g. a = 1. We are interested only in the fill-height range $0 < h_V < b/a$, i.e. only in volumes that are smaller than that of the annular crevice at the container bottom.

Before describing our computational algorithm in detail we shall give the explicit form of the boundary conditions (2.21) at $s = s_0$ and $s = s_1$, respectively. In a neighborhood of $s = s_0$ there holds by (2.3), since the bottom is an ellispoid of revolution (cf. Figs.1 and 2)

$$\frac{(R(s) - w(s)Z'(s))^2}{a^2} + \frac{(Z(s) + w(s)R'(s))^2}{b^2} = 1 . \quad (3.2)$$

Similarly, in a neighborhood of $s = s_1$ we have

$$R(s) - w(s)Z'(s) = a . \quad (3.3)$$

By differentiating these expressions twice and using (2.9), (2.21) becomes after some straightforward manipulations (we put $Z_i = Z(s_i)$, $R_i = R(s_i)$, $i = 0, 1$, for brevity)

$$\sin\gamma\cdot\mu'(s_0) = \left\{\frac{a^4b^4}{(a^4Z_0^2 + b^4R_0^2)^{3/2}} + \cos\gamma\cdot(BZ_0 - H - \frac{Z_0'}{R_0})\right\}\cdot\mu(s_0) , \quad (3.4)$$

$$\sin\gamma\cdot\mu'(s_1) = -\cos\gamma\cdot(BZ_1 - H - \frac{\cos\gamma}{a})\,\mu(s_1) . \quad (3.5)$$

Our computations are carried out for the case $b/a = 0.724$ and proceed in two principal steps. In the first of these (which requires the main part of the computational effort) we determine successively some 50-60 points on the curve $B_{0c} = B_{0c}(h_V)$ at non-equidistant values of h_V. Each of these points is obtained in the following manner:

a) We choose a fixed point $R = a = 1$, $Z = Z_1$ at the cylindrical container wall and "guess" a corresponding pair of values for B_0 and H_0 in a way to be specified below.

b) We put $R(s_1) = a = 1$, $Z(s_1) = Z_1$, $R'(s_1) = \sin\gamma$, $Z'(s_1) = \cos\gamma$ to satisfy the boundary conditions at $s = s_1$ in (2.9) (we may choose s_1 arbitrarily, e.g. $s_1 = 1$). We further choose a pair of values $\mu'(s_1)$, $\mu(s_1)$, not both zero, consistent with the boundary condition

(3.5) (except for the large h_V cases for $\gamma = 0$, cf. (3.6) below).

c) We solve simultaneously the differential equations (2.9) and (2.20) numerically, integrating from $s = s_1$ backwards with a standard fourth-order Runge-Kutta scheme. The stepsize of the integration is kept constant except for the last step which is adjusted (using a secant method) so as to make the last computed point of the solution to (2.9) lie on the container bottom profile (for the case $\gamma = 0$ we adjust the last step so as to make the normal of the computed solution to (2.9) at $s = s_0$ intersect the bottom profile at an angle of $\pi/2$). Thus we have ensured $w(s_0) = 0$ ($w'(s_0) = 0$ in the case $\gamma = 0$).

d) We compute the discrepancies in the boundary condition (3.4) and the remaining boundary condition at $s = s_0$ in (2.9). We adjust B_0 and H_0 (using eventually a Newton-type method to obtain the corrections) and repeat from b) above until the corrections in B_0 and H_0 are less than a prescribed tolerance.

e) We make a final integration computing this time also the liquid volume V, simply by adding the appropriate extra differential equation to the others. Then the corresponding h_V-value is obtained using (3.1).

We repeat the steps a)-e), using a set of some 50-60 regularly spaced Z_1-values. To obtain the initial "guesses" for B_0 and H_0 in a), we extrapolate the functions $B_{0c} = B_{0c}(Z_1)$ and $H_{0c} = H_{0c}(Z_1)$ to the next Z_1-value, fitting two quadratic polynomials in Z_1 through the three closest previously computed values of $\log|B_{0c}|$ and $\log|H_{0c}|$, respectively.

The functions $\log|B_{0c}(Z_1)|$ and $\log|H_{0c}(Z_1)|$ turn out to be close to linear in Z_1, and the accuracy in the guessed values was found to be very good (the "guesses" have in general 3-4 correct decimals when the spacing of the Z_1-values is 0.02a).

For all the contact angles studied, the computed points on the curve $B_{0c} = B_{0c}(h_V)$ indicate that $\log|B_{0c}|$ is only mildly nonlinear as a function of h_V. The second main step of our computation is to fit a cubic spline through the computed points on the curve $\log|B_{0c}| = \log|B_{0c}(h_V)|$. In this way we obtain a convenient and satisfactorily accurate representation of the sought function $B_{0c} = B_{0c}(h_V)$ throughout the entire h_V-interval of interest.

We have studied the contact angle values $\gamma = 4°$, $2°$, $1°$, and $0°$, the last of these values being the case of main interest. In the case $\gamma = 0$ we find that the above algorithm must be modified in the following way: When, in step a) above, $Z_1 > Z_1^*$ (corresponding to $h_V > h_V^*$, where $Z_1^* = 0.7014$ and $h_V^* = 0.5031$ with four correct decimals), then the condition

$$w''(s_1) \leqslant 0 \tag{3.6}$$

(which expresses the condition that the equilibrium liquid-vapor interface must lie inside the container for $s < s_1$, cf. the discussion at the end of Section 2) places a more restrictive bound on B_0 than the conditions under d) above. By (3.3), (3.6) is equivalent to

$$R''(s_1) = -(B_0 Z_1 - H_0 - 1) \leqslant 0 \quad . \tag{3.7}$$

Hence, when $\gamma = 0$ and $Z_1 > Z_1^*$ we solve, in steps b) and c) above, only the differential equations (2.9) and adjust, in step d), B_0 and H_0 so as to satisfy $w(s_0) = 0$ and $B_0 Z_1 - H_0 - 1 = 0$ (using again a Newton-like method obtain the corrections).

4. NUMERICAL RESULTS

Table 1 shows the cubic spline approximations to the functions $B_{0c} = B_{0c}(h_V)$ for the contact angle values $\gamma = 0°$, $1°$, $2°$, and $4°$ (for the case b/a = 0.724). The relative error in each entry shown is less than 10^{-4}, as estimated from repeated computations with different stepsizes in the numerical integration and different spacings for the Z_1-values used in step a) in the computational algorithm (cf. Section 3).

Figures 3-6 show graphs of the functions in Table 1. For practical resons we use a logarithmic scale on the B_{0c}-axis, for which the curves are close to linear. Figure 7, showing all the graphs from Figures 3-6 simultaneously, illustrates the almost insignificant dependence on γ in this range.

In Figure 8 we show the equilibrium surfaces at critical Bond number for the fill heights $h_V = 0.2(0.1)0.7$ for the case $\gamma = 0°$. The curves were plotted by numerical integration from starting points at the cylindrical wall using the subroutine package GRAFPAC available at LBL for graphical display of the results. The starting points for the integrations were obtained using cubic spline fitting to the points on the curve $Z_1 = Z_1(h_V)$, which are known as a "by product" of the $B_{0c} = B_{0c}(h_V)$ - calculation (cf. steps a) - e) of the algorithm described in Section 3).

The graphs of Figure 9 represent solutions to the Jacobi-Legendre equation (2.20) in the cases corresponding to the equilibrium configurations shown in Figure 8. The functions shown in Figure 9 are of the form

$$\nu(s) = \frac{\mu(s)}{R'(s)} \tag{4.1}$$

where $\mu(s)$ is a solution to (2.20) satisfying $\mu(s_0) = 0$. The function $\nu(s)$ depicts the radial dependence of the perturbation $\mu(s)\cos\phi$, but in terms of vertical displacement (whereas $\mu(s)$ is the radial perturbation profile in terms of displacement normal to the unperturbed surface, cf. (2.2)). The abscissa of the graphs in Figure 9 is R(s) and the functions are normalized so that $d\nu/dR \approx 1$ at the left end points. Theoretically, for $h_V > h_V^* \approx 0.5031$ (see (3.6)) the functions $\nu(s)$ defined in (4.1) have a singularity at $s = s_1$, i.e. at $R = 1$, while for $h_V < h_V^*$ $\nu(s_1)$is nonzero but finite. Hence the graph corresponding to $h_V = 0.5$ in Figure 9 in fact intersects the line $R = 1$, whereas the two graphs above it do not.

Finally, in Figures 10-15 we show the equilibrium liquid-vapor interfaces of Figure 8 (solid lines) together with the equilibrium liquid-vapor interfaces superimposed by a small multiple of the corresponding $\nu(s)$ as given by (4.1). These curves are of some interest because, theoretically, when $B_0 = B_{0c}$ and $h_V < h_V^*$ the only possible initial shape of an unstable perturbation is given by $\nu(s)\cos\phi$ (in terms of vertical displacement). For $h_V > h_V^*$ it can in fact be shown (Karasalo [5]) that the configurations are unstable at $B_0 = B_{0c}$ for

e.g. perturbations that build up some suitably chosen, axially symmetric layer of liquid above the unperturbed contact line at the cylindrical wall. Notice, however, that the dashed curves in Figures 14 and 15 do not show such a perturbation, but they are nevertheless included here for completeness. These results on the initial perturbation shape rely, of course, on several idealizing assumptions, such as that (1.1) holds exactly, that it represents all boundary constraints, that viscosity effects need not be included, etc., and the conclusions from Figures 10-15 should not be drawn too far.

The numerical results presented here have been found to be consistent with preliminary experimental results obtained at the NASA Lewis Research Center [6].

5. ACKNOWLEDGEMENTS

We wish to thank Eugene P. Symons for initiating our interest in this problem by means of the remarkable color movies of stability experiments carried out at the NASA Lewis Zero Gravity Facility for the container depicted in Fig. 1, and for his continued interest and sharing of experimental data with us during the course of our study. This work was supported in part by the National Aeronautics and Space Administration and by the Energy Research and Development Administration.

REFERENCES

1. R.F. Lacovic, Centaur zero gravity coast and engine restart on the Titan/Centaur (TC-2) extended mission, NASA TM X - 71821, Lewis Research Center, Cleveland, Ohio, October 1975.

2. P. Concus, G.E. Crane, H.M. Satterlee, Small amplitude lateral sloshing in spheroidal containers under low gravitational conditions. NASA CR - 72500 Lewis Research Center, Cleveland, Ohio, February, 1969.

3. N. Abramson (editor), The dynamic behavior of liquid in moving containers, NASA SP 106, U.S. Government Printing Office, Washington D.C., 1966.

4. I. Karasalo, Sufficient conditions for stability of axisymmetric annular fluid interfaces, LBL 4898, Lawrence Berkeley Laboratory, Berkeley, California, June 1976.

5. I. Karasalo, Stability of axisymmetric, annular fluid interfaces at zero contact angle, Preprint LBL 5318, Lawrence Berkeley Laboratory, Berkeley, California, June 1976 (to appear in Arch. Rat. Mech. Anal.).

6. E.P. Symons (private communication), 1976.

Table 1. Critical Bond number, B_{0c}, as function of fill height, h_V, at $\gamma = 0°$, 1°, 2°, and 4°.

h_V	$\gamma = 0°$	$\gamma = 1°$	$\gamma = 2°$	$\gamma = 4°$
0.200	-480.4283	-480.3526	-480.1183	-479.1676
0.210	-412.6934	-412.6251	-412.4212	-411.5999
0.220	-356.8787	-356.8212	-356.6472	-355.9423
0.230	-310.4444	-310.3955	-310.2463	-309.6393
0.240	-271.5210	-271.4787	-271.3503	-270.8253
0.250	-238.6539	-238.6178	-238.5075	-238.0536
0.260	-210.7102	-210.6795	-210.5850	-210.1928
0.270	-186.8042	-186.7783	-186.6978	-186.3599
0.280	-166.2339	-166.2123	-166.1443	-165.8546
0.290	-148.4377	-148.4200	-148.3635	-148.1170
0.300	-132.9638	-132.9499	-132.9038	-132.6967
0.310	-119.4456	-119.4352	-119.3990	-119.2280
0.320	-107.5834	-107.5765	-107.5497	-107.4123
0.330	-97.1310	-97.1274	-97.1098	-97.0041
0.340	-87.8844	-87.8843	-87.8757	-87.8004
0.350	-79.6741	-79.6776	-79.6781	-79.6321
0.360	-72.3581	-72.3654	-72.3752	-72.3581
0.370	-65.8171	-65.8287	-65.8482	-65.8598
0.380	-59.9504	-59.9666	-59.9965	-60.0369
0.390	-54.6722	-54.6937	-54.7349	-54.8046
0.400	-49.9096	-49.9374	-49.9908	-50.0906
0.410	-45.6000	-45.6353	-45.7024	-45.8332
0.420	-41.6896	-41.7341	-41.8166	-41.9796
0.430	-38.1320	-38.1879	-38.2878	-38.4843
0.440	-34.8869	-34.9574	-35.0769	-35.3082
0.450	-31.9190	-32.0084	-32.1502	-32.4173
0.460	-29.1976	-29.3120	-29.4786	-29.7822
0.470	-26.6956	-26.8433	-27.0371	-27.3775
0.480	-24.3887	-24.5813	-24.8043	-25.1807
0.490	-22.2554	-22.5086	-22.7615	-23.1725
0.500	-20.2759	-20.6107	-20.8925	-21.3355
0.510	-18.4509	-18.8751	-19.1830	-19.6544
0.520	-16.8150	-17.2908	-17.6204	-18.1156
0.530	-15.3484	-15.8474	-16.1930	-16.7068
0.540	-14.0314	-14.5345	-14.8900	-15.4170
0.550	-12.8467	-13.3417	-13.7013	-14.2359
0.560	-11.7792	-12.2587	-12.6174	-13.1545
0.570	-10.8157	-11.2756	-11.6291	-12.1641
0.580	-9.9447	-10.3828	-10.7281	-11.2570
0.590	-9.1561	-9.5717	-9.9065	-10.4259

Table 1. (cont.)

0.600	-8.4411	-8.8342	-9.1571	-9.6644
0.610	-7.7920	-8.1630	-8.4730	-8.9662
0.620	-7.2017	-7.5517	-7.8483	-8.3259
0.630	-6.6644	-6.9942	-7.2773	-7.7384
0.640	-6.1746	-6.4854	-6.7551	-7.1990
0.650	-5.7276	-6.0204	-6.2770	-6.7035
0.660	-5.3192	-5.5951	-5.8390	-6.2481
0.670	-4.9456	-5.2057	-5.4373	-5.8291
0.680	-4.6035	-4.8487	-5.0686	-5.4435
0.690	-4.2898	-4.5212	-4.7299	-5.0884
0.700	-4.0020	-4.2204	-4.4185	-4.7610

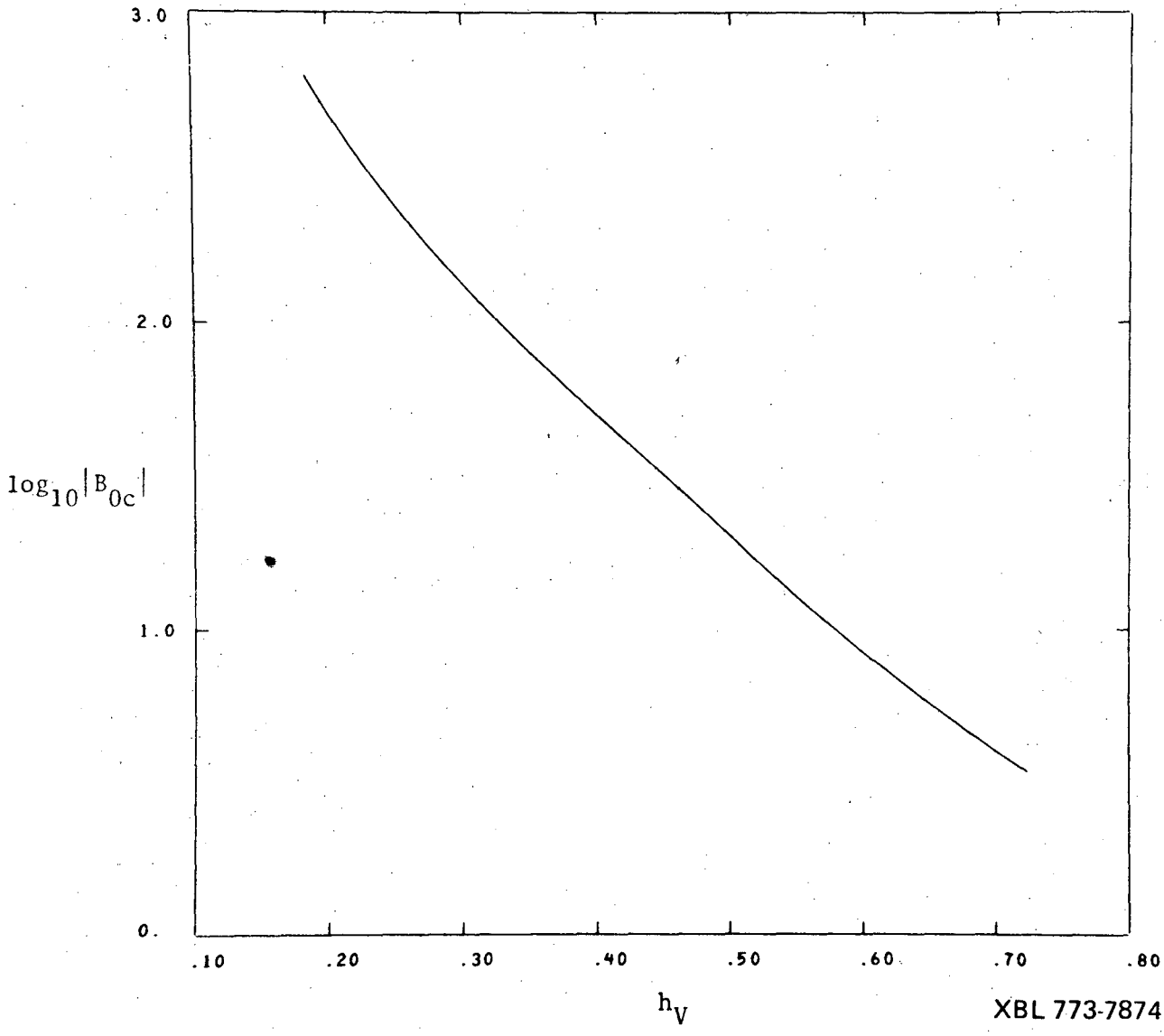

Figure 3: B_{0c} as a function of h_V for $\gamma = 0°$.

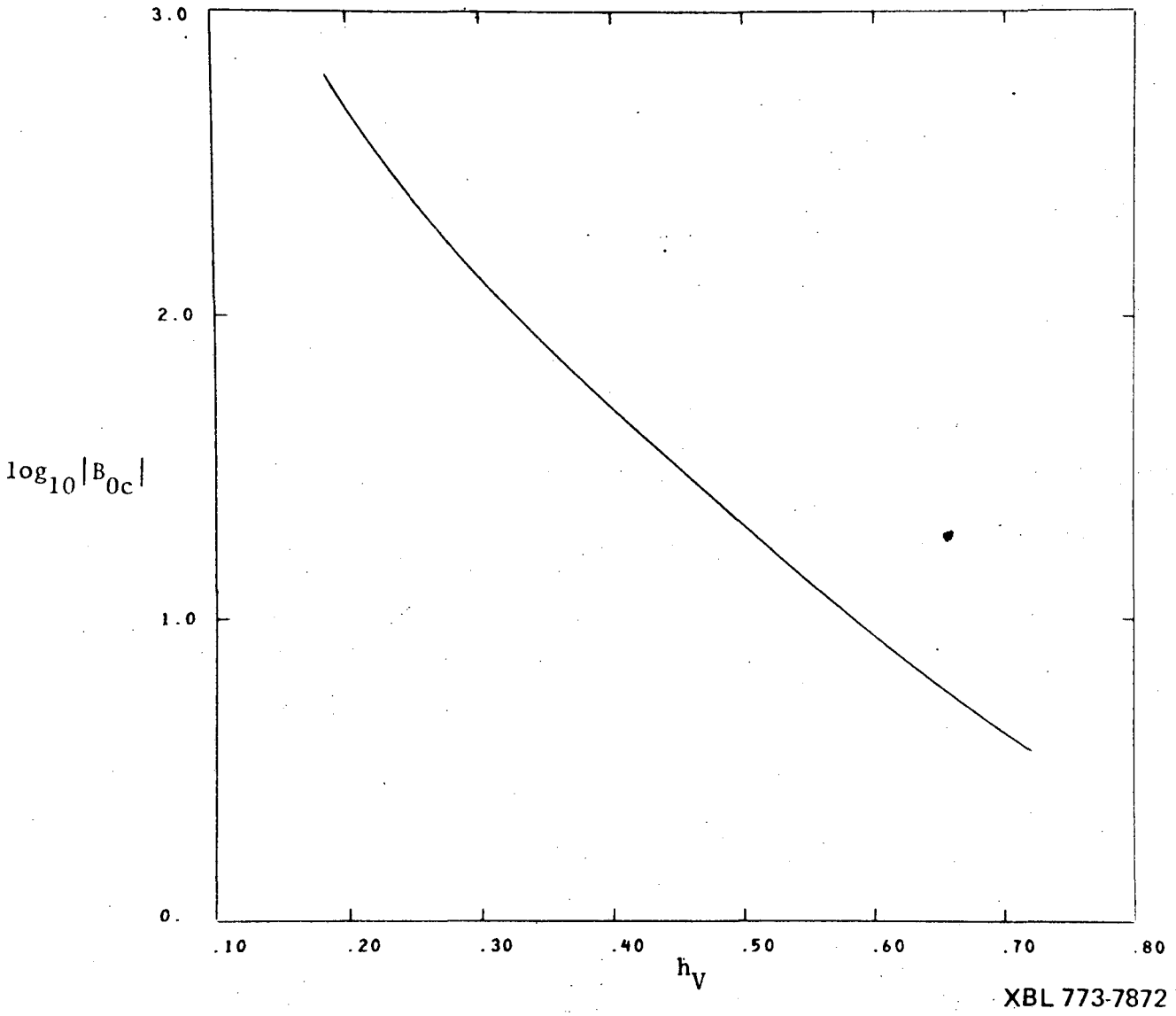

Figure 4: B_{0c} as a function of h_V for $\gamma = 1°$.

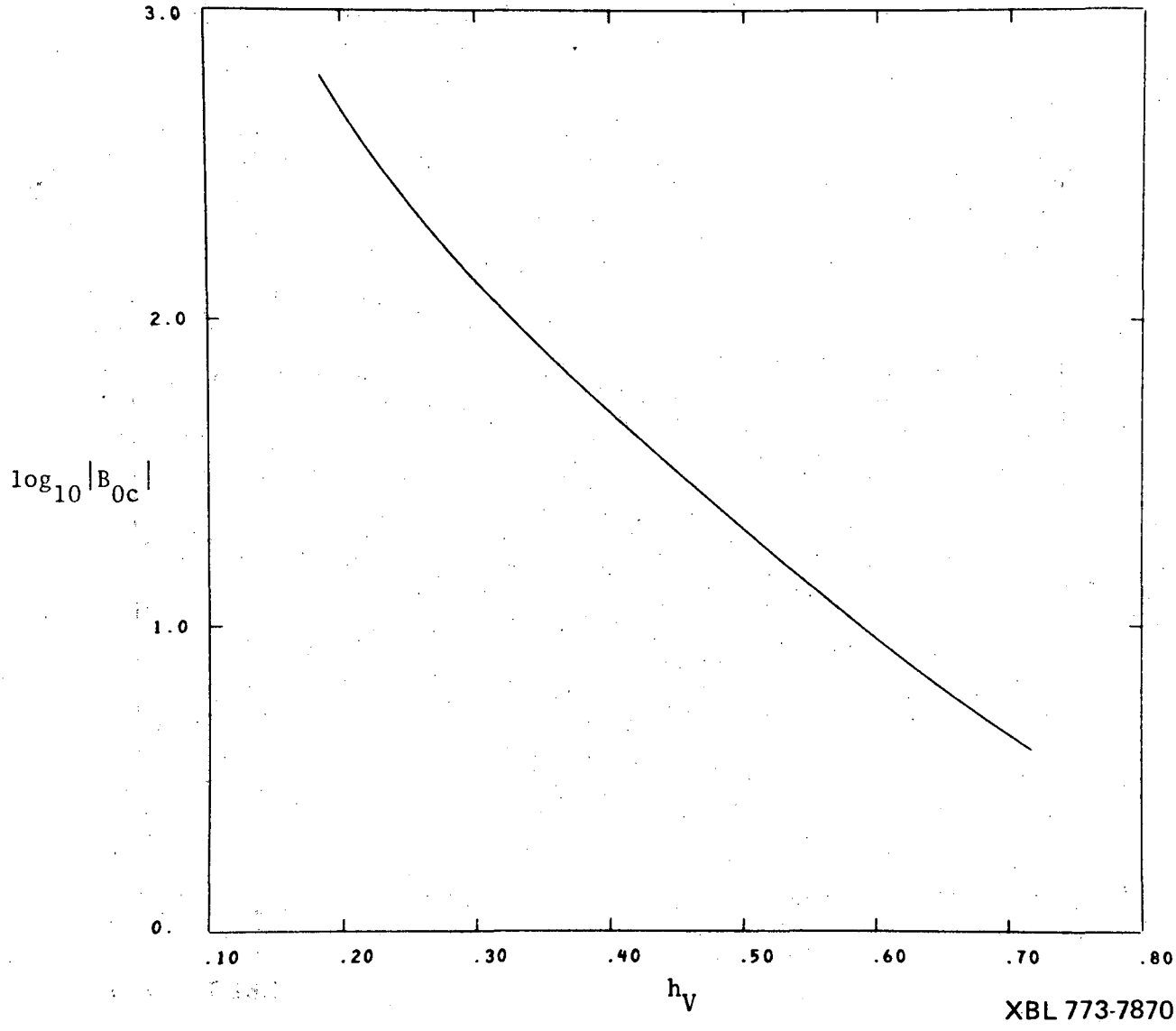

Figure 5: B_{0c} as a function of h_V for $\gamma = 2°$.

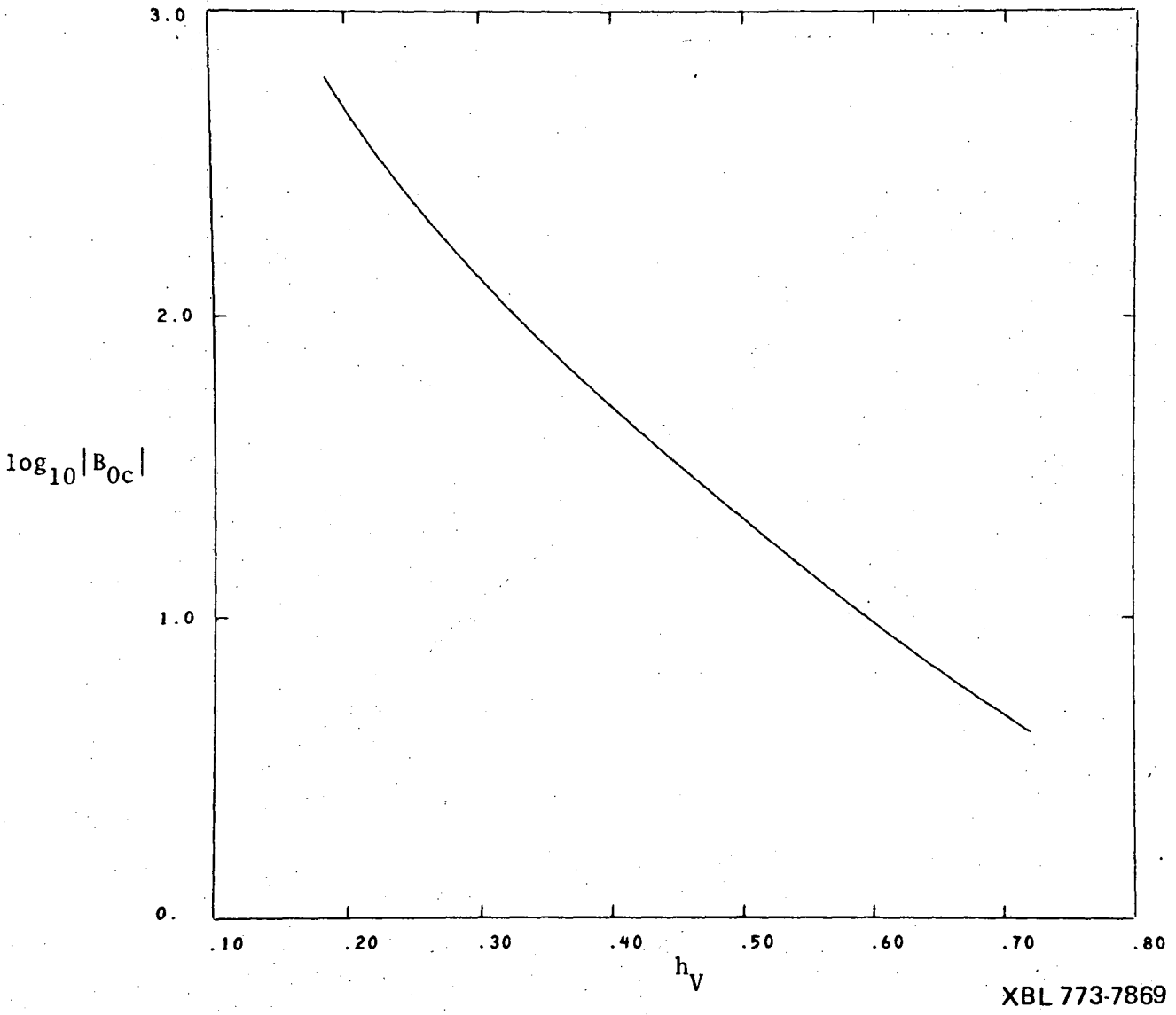

Figure 6: B_{0c} as a function of h_V for $\gamma = 4°$.

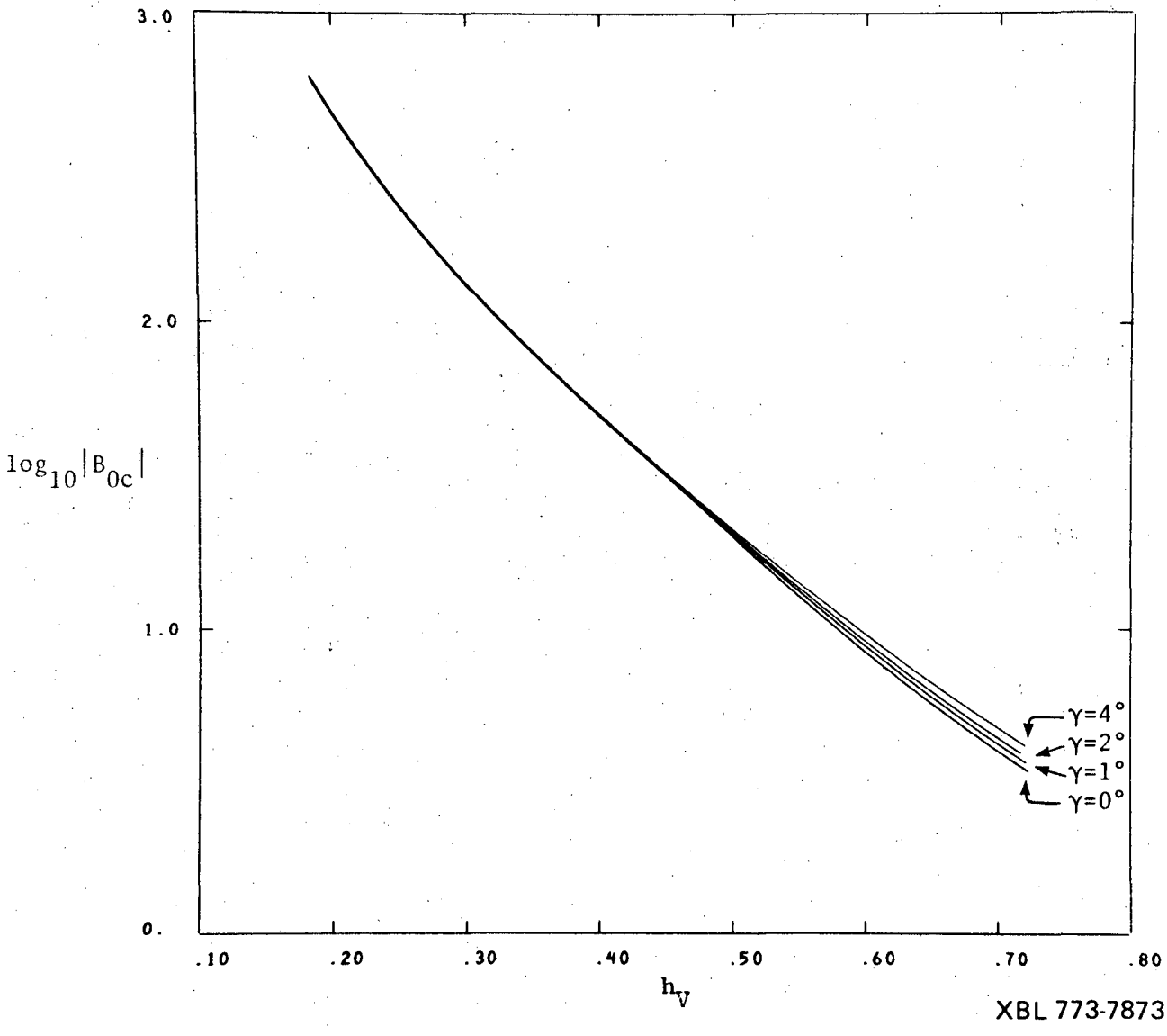

Figure 7: B_{0c} as a function of h_V for γ = 0°, 1°, 2° and 4°.

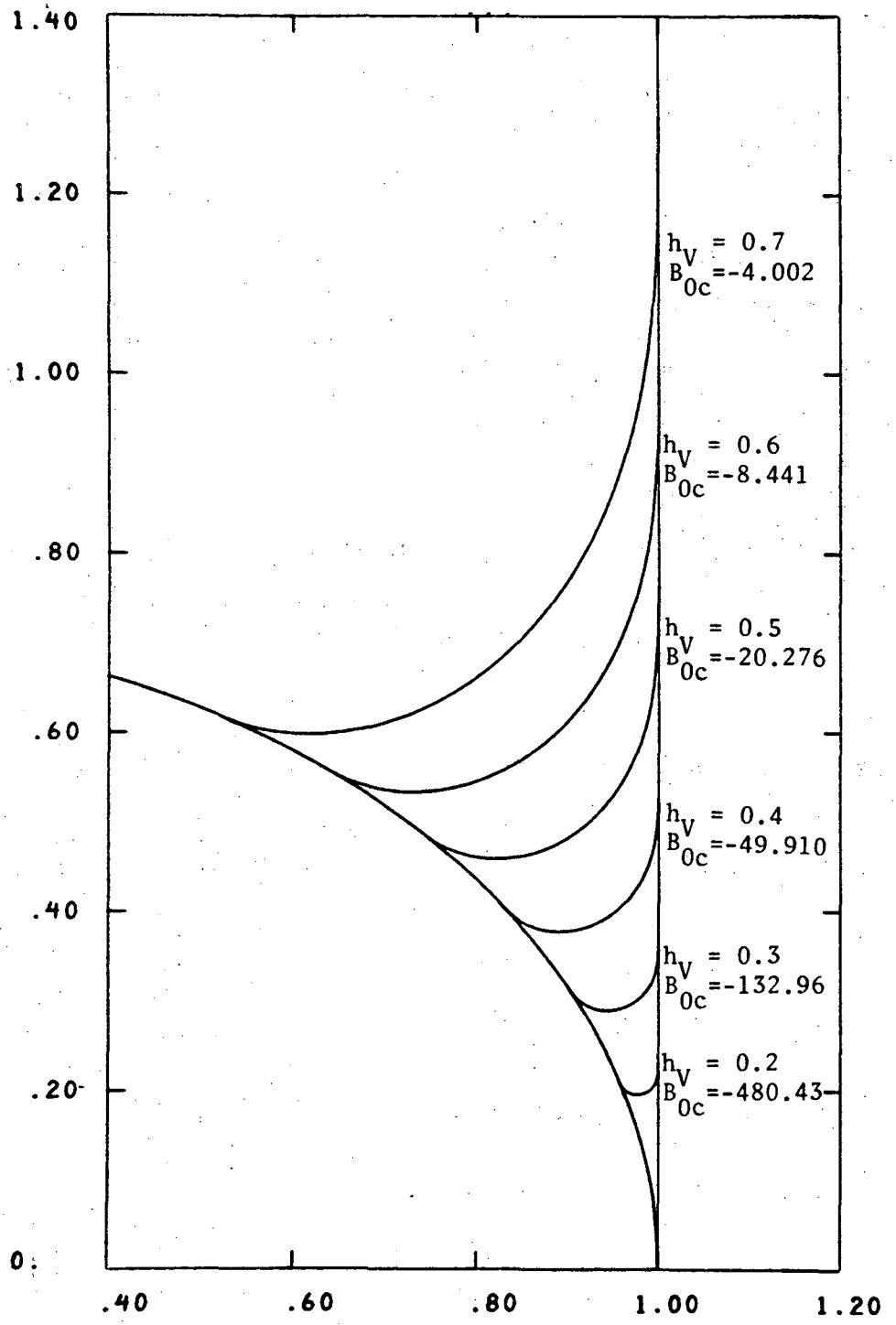

Figure 8: Equilibrium surfaces at critical Bond number for $\gamma = 0°$.

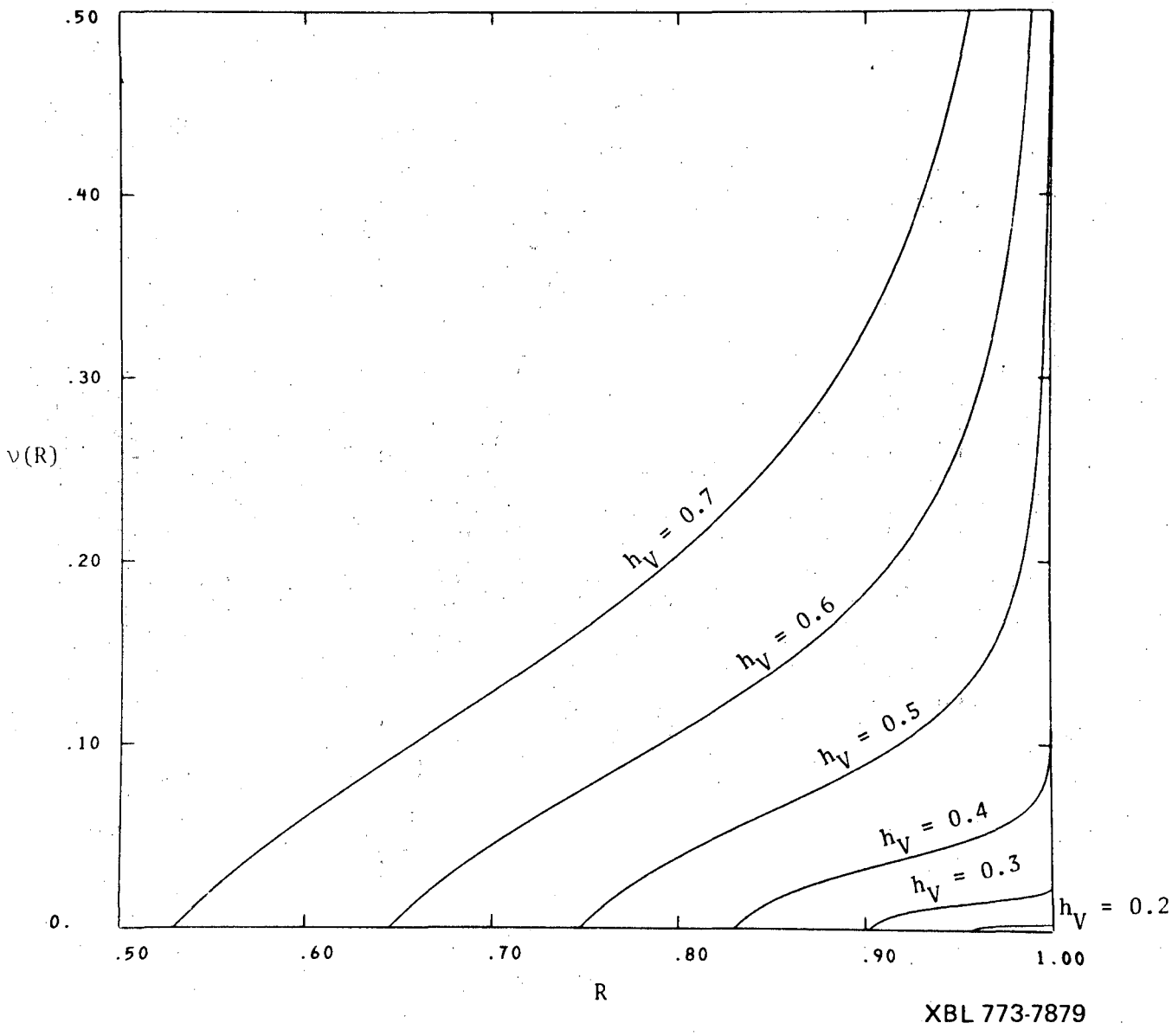

Figure 9: Radial dependence of first angular perturbation modes in terms of vertical displacement. Curves normalized so that $\gamma(R_o) = 0$ and $(\frac{d\gamma}{dR})_{R_o} = 1$. ($R_o$ = left end point of curve.)

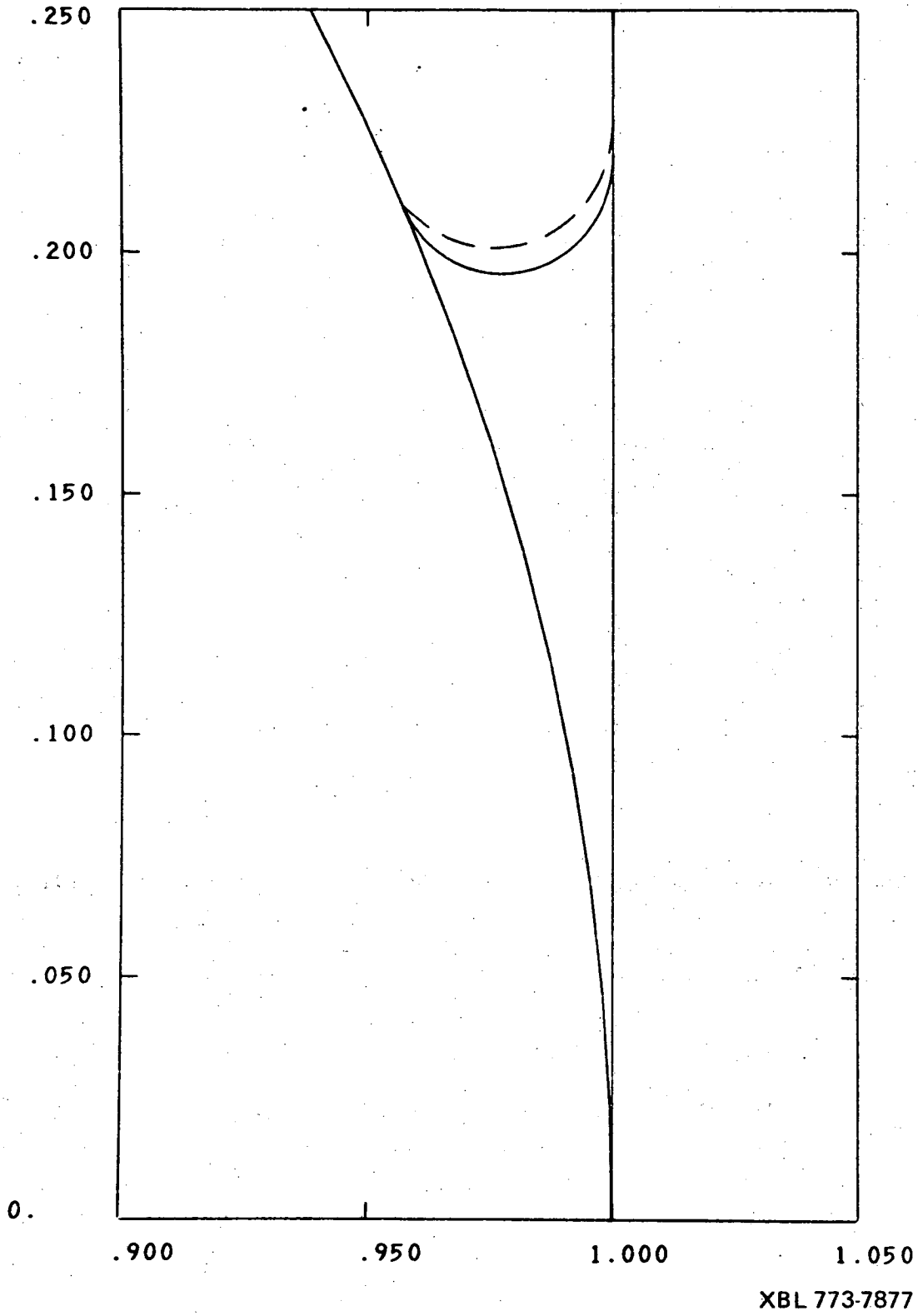

Figure 10: Solid Curve: Equilibrium surface at critical Bond number for $\gamma = 0°$ and $h_V = 0.2$.

Dashed Curve: Solid curve superimposed with the corresponding perturbant mode from Figure 9.

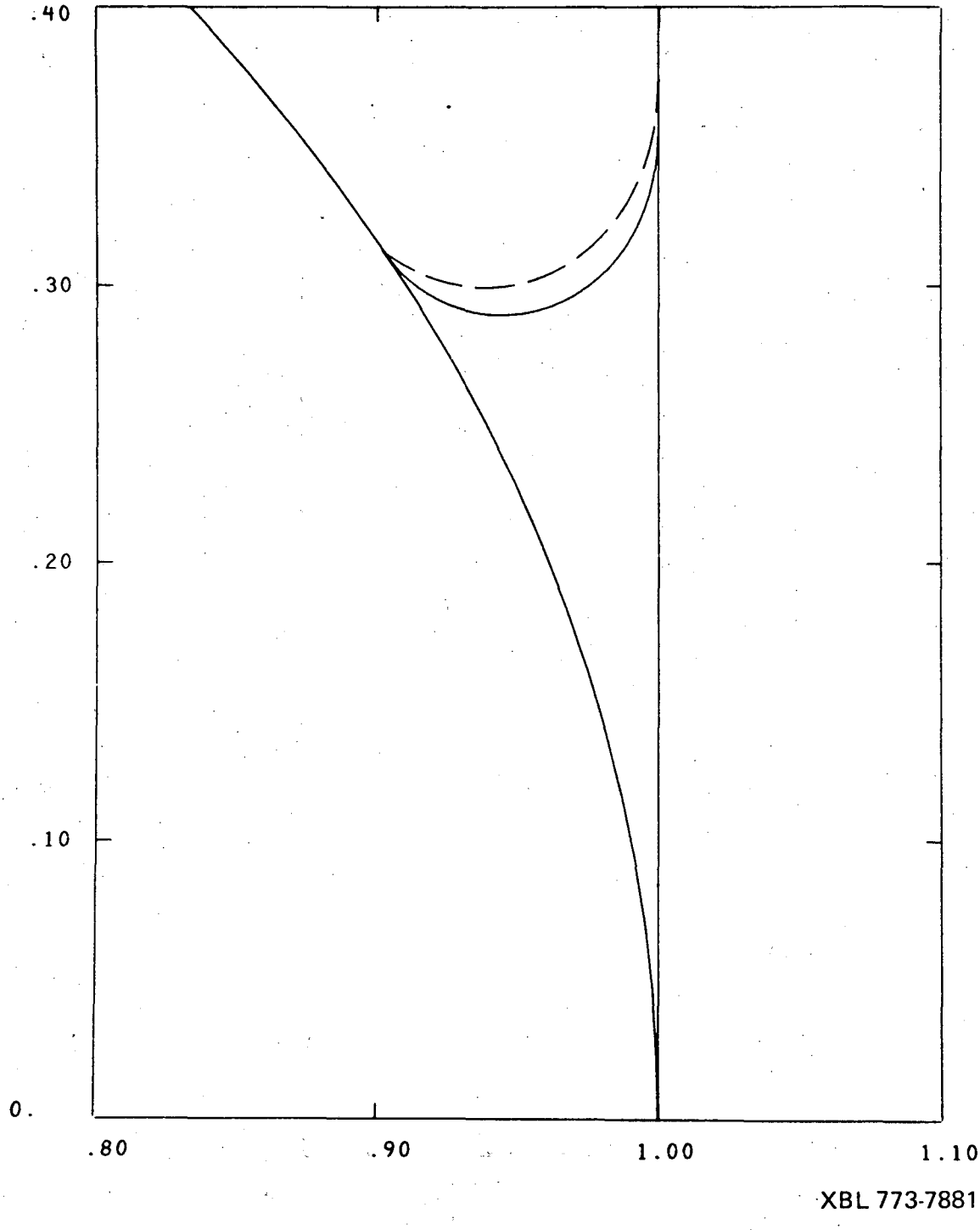

Figure 11: Solid Curve: Equilibrium surface at critical Bond number for $\gamma = 0°$ and $h_V = 0.3$.

Dashed Curve: Solid curve superimposed with the corresponding perturbation mode from Figure 9.

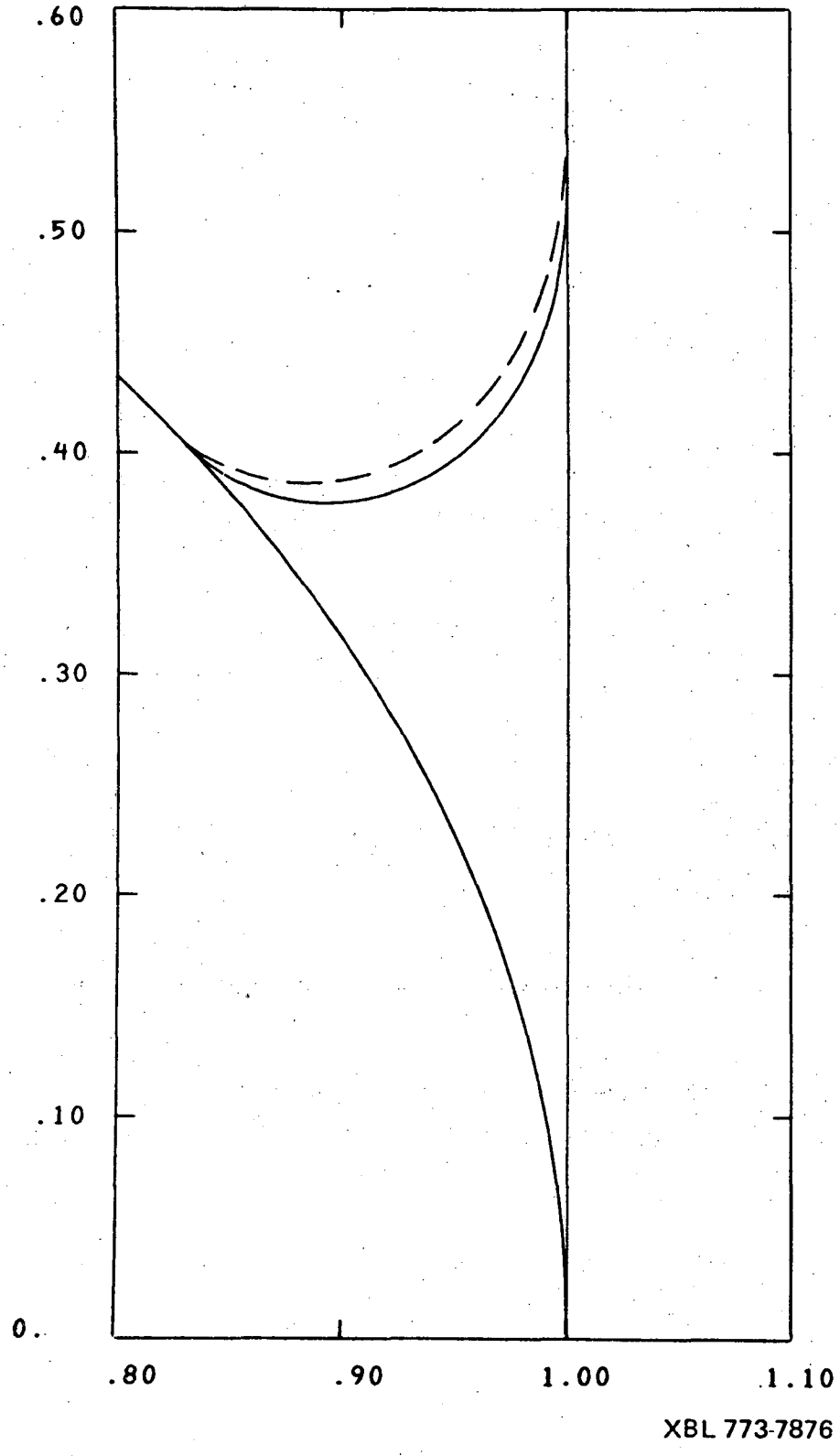

Figure 12: Solid Curve: Equilibrium surface at critical Bond number for $\gamma = 0°$ and $h_V = 0.4$.

Dashed Curve: Solid curve superimposed with the corresponding perturbation mode from Figure 9.

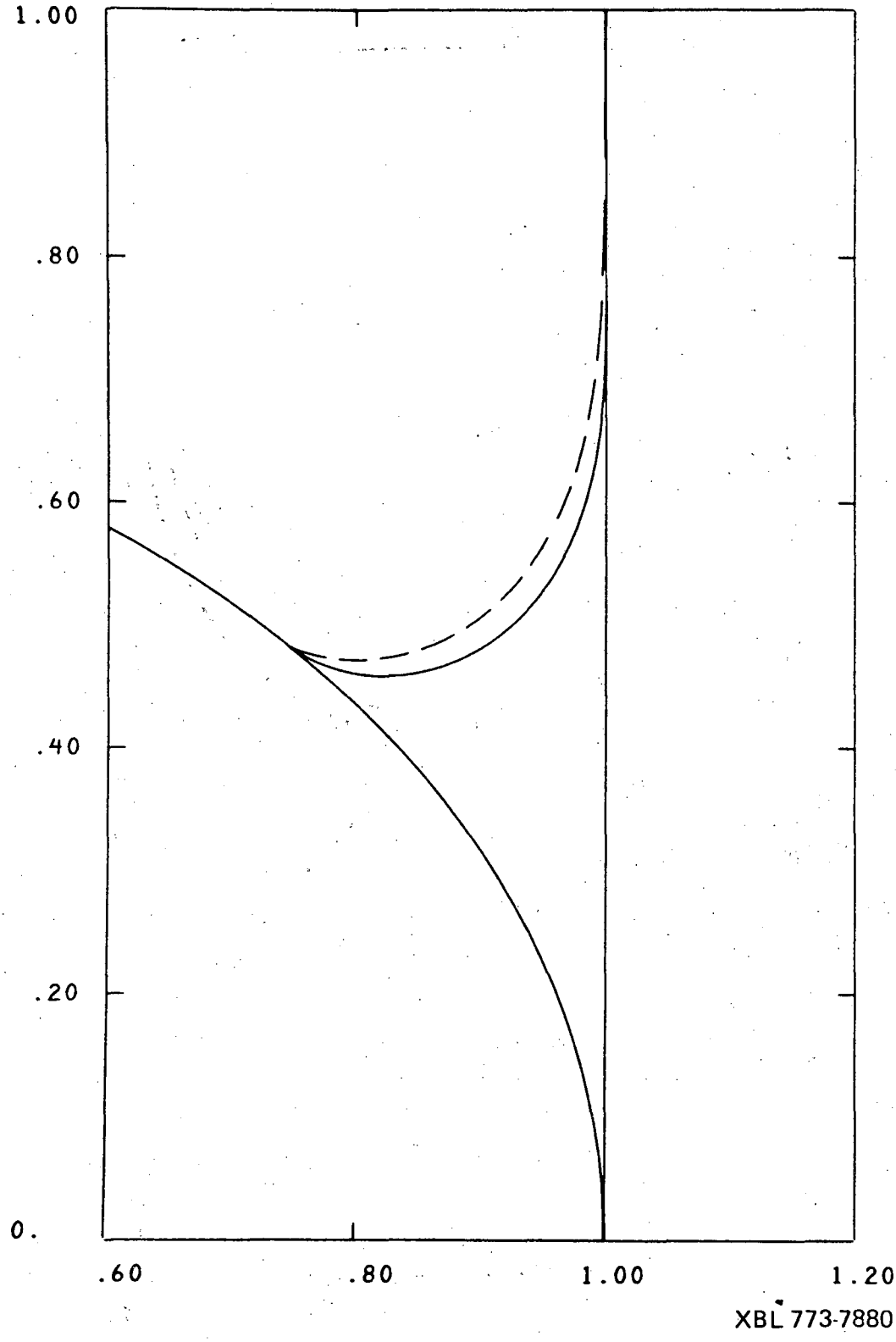

Figure 13: Solid Curve: Equilibrium surface at critical Bond number for $\gamma = 0°$ and $h_V = 0.5$.

Dashed Curve: Solid curve superimposed with the corresponding perturbation mode from Figure 9.

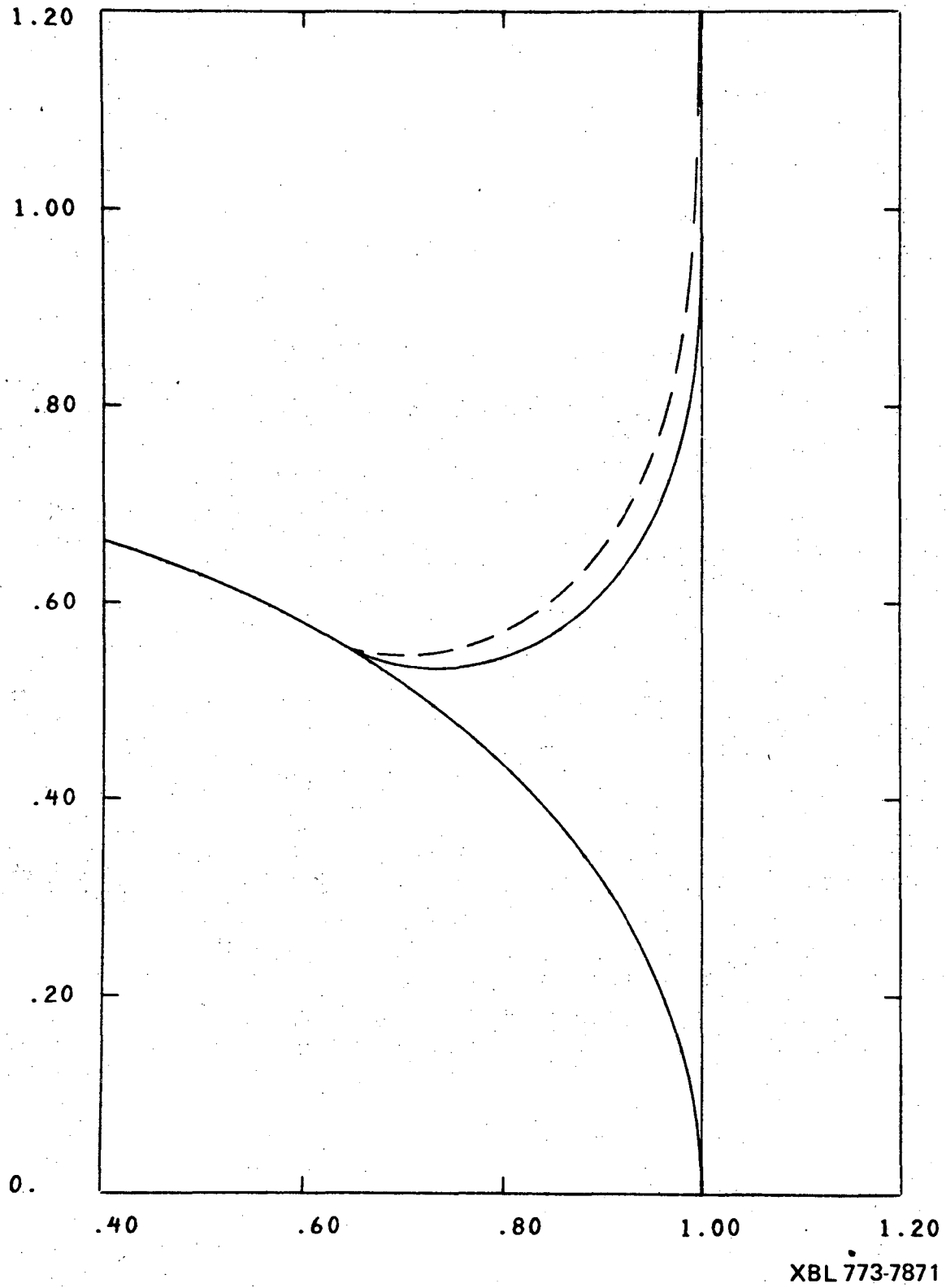

Figure 14: Solid Curve: Equilibrium surface at critical Bond number for $\gamma = 0°$ and $h_V = 0.6$.

Dashed Curve: Solid curve superimposed with the corresponding perturbation mode from Figure 9.

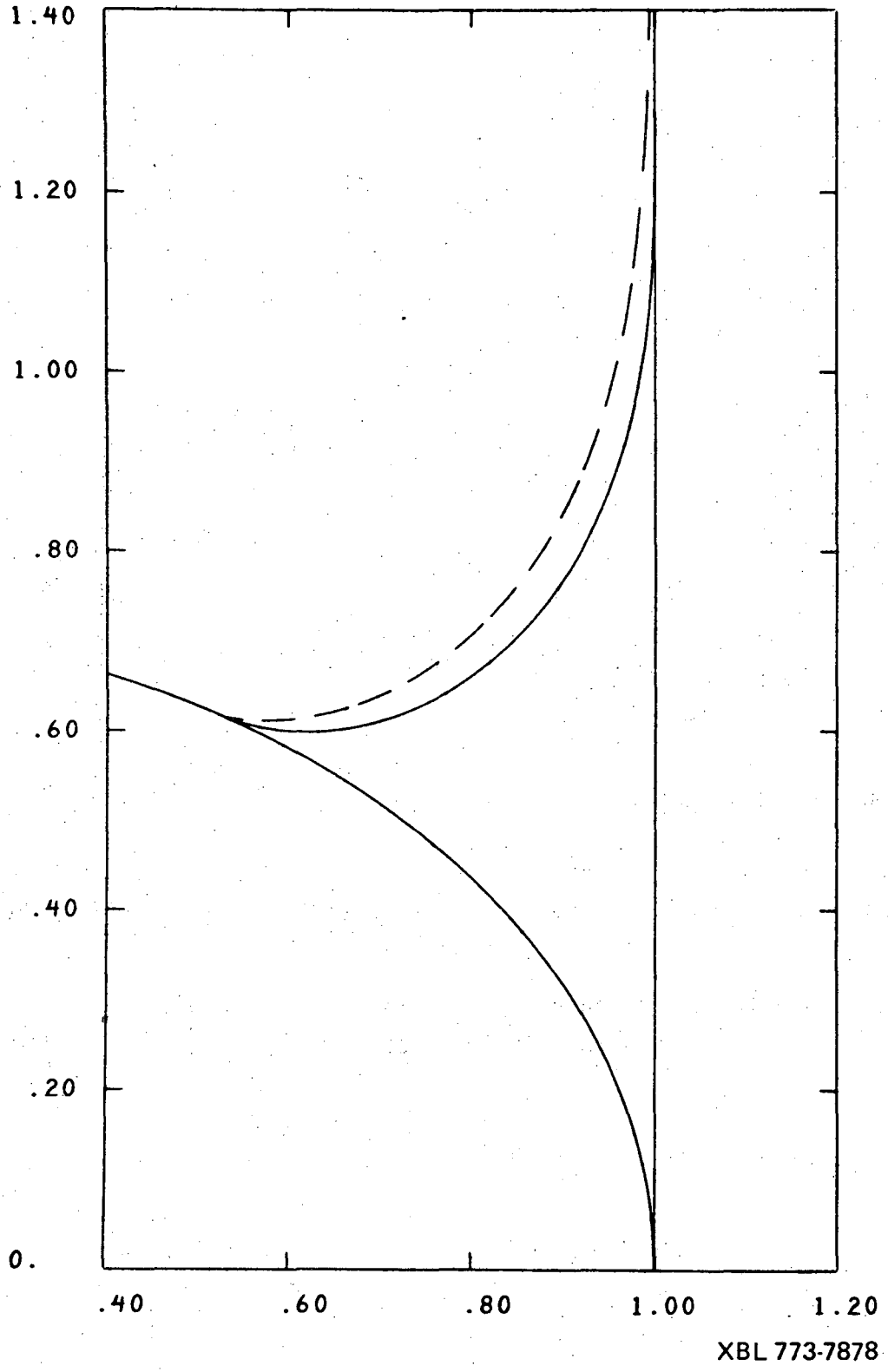

Figure 15: Solid Curve: Equilibrium surface at critical Bond number for $\gamma = 0^\circ$ and $h_V = 0.7$.

Dashed Curve: Solid curve superimposed with the corresponding perturbation mode from Figure 9.

TECHNICAL INFORMATION DIVISION
LAWRENCE BERKELEY LABORATORY
UNIVERSITY OF CALIFORNIA
BERKELEY, CALIFORNIA 94720